Influence of a longitudinal field on the large in-plane nuclear field formation in single quantum dots

S. Yamamoto[1] T. Arakawa[2], R. Matsusaki[1], R. Kaji[1], S. Adachi[*,1]

[1] Division of Applied Physics, Graduate School of Engineering, Hokkaido University, Sapporo 060-8628, Japan
[2] Applied Physics and Engineering Course, Faculty of Engineering, Hokkaido University, Sapporo 060-8628, Japan

Received XXXX, revised XXXX, accepted XXXX
Published online XXXX

Key words: quantum dot, hyperfine interaction, nuclear quadrupole interaction.

[*] Corresponding author: e-mail adachi-s@eng.hokudai.ac.jp, Phone: +81-11-7066709, Fax: +81-11-7066709

Experimental studies on the role of nuclear quadrupole interaction to the in-plane nuclear field formation were carried out in single self-assembled $In_{0.75}Al_{0.25}As/Al_{0.3}Ga_{0.7}As$ quantum dots. In Hanle effect measurements, the electron depolarization curves apart far from a standard Lorentzian shape were observed: the curves with anomalously large width and hysteretic behavior at the critical transverse magnetic field. These anomalies indicated the growth of an in-plane nuclear field compensating the applied transverse magnetic field up to $\sim$1 T and appeared regardless of the excitation helicity. The azimuth angle dependence of the critical field of the hysteretic response revealed that the principal axis of the nuclear quadrupole interaction is almost parallel to the crystal growth axis. This fact suggests that the main origin of the nuclear quadrupole interaction which is related with in-plane nuclear field formation is not random alloying among In and Al nuclei but residual strain of quantum dots. Further, a longitudinal magnetic field by a neodymium magnet broke the excitation-helicity independence of the Hanle curves and the shape of curves became very different depending on the helicity. The obtained results were explained well with a simple consideration and indicated that the nuclear quadrupole interaction takes multirole in the formation of in-plane nuclear field.

1 Introduction Hyperfine interaction (HFI), a magnetic interaction between an electron spin and nuclear spins, has significant importance on the spin dynamics especially in quantum nanostructures such as quantum dots (QDs) [1–3]. This is because an electron spin and spins of lattice nuclei in a localized volume form a strongly coupled system via the HFI. In this system, the angular momentum of the injected electron spin polarization can be easily transferred via the HFI onto the nuclear subsystem where the spin polarization may be preserved for a long time. Since the nuclear spin polarization (NSP) not only has the possibility for various applications such as a quantum memory [4–8] but also affects the electron spin states as a nuclear field [2,3], it is important to reveal the formation and relaxation mechanisms of NSP entirely.

Recently, a large nuclear field orthogonal to the photo-injected electron spin has been reported in the self-assembled (SA) InAs and InAlAs QDs [9–12], which is beyond the scope of a traditional model [1] where a large nuclear field parallel to the injected electron spin was mainly discussed. Such a large *in-plane* nuclear field induces a drastic distortion of the electron spin depolarization curve under the transverse magnetic field (i.e. Hanle curve), while *W-shaped* Hanle curve in a strain-free $GaAs/Al_{0.3}Ga_{0.7}As$ QD was reproduced reasonably with the traditional model [13]. These studies suggest strongly that the nuclear quadrupole interaction (NQI), which is caused from the coupling of nuclear spin and electric field gradient induced by the residual strain in SA-QDs, contributes to the formation of a large in-plane nuclear field. To date, we have proposed a formation model of the large

in-plane nuclear field by considering the effects of NQI and successfully obtained a qualitative agreement with the observed anomalous Hanle curves [11, 12]. In the model, two effects; the stabilization of NSP along the principal axis of NQI and strongly anisotropic response of nuclear states due to the eigenstate mixing, are included as the effects of NQI.

In this study, we focus on the role of NQI and extend the experiments as follows; First, the azimuth angle dependence of nuclear field provides the information about the characteristic axis of NQI. Next, a longitudinal magnetic field comparable to the strength of NQI is introduced in the Hanle effect measurements, which affects the effects of NQI.

2 Sample and experimental apparatus The single SA $In_{0.75}Al_{0.25}As/Al_{0.3}Ga_{0.7}As$ QDs grown by molecular beam epitaxy on a (100)-GaAs substrate were used in this study. After fabrication of small mesa structures, micro-photoluminescence (μ-PL) measurements were carried out. A continuous-wave Ti:sapphire laser was tuned to provide the transition energy to the band edge of the wetting layer ($\lambda\sim730$ nm). From atomic force microscopy measurements of a reference uncapped QD layer and cross-section transmission electron microscope observation, the QDs have a lens-shaped profile with typical diameter of $\sim$ 20 nm and height of $\sim$4 nm, and the number of nuclei in a single QD is estimated as $N\sim3\times10^4$ [14].

Figure 1(a) is typical PL spectra from exciton complexes of a single QD under non-polarized excitation at 6 K and zero magnetic field. The PL spectra indicated by

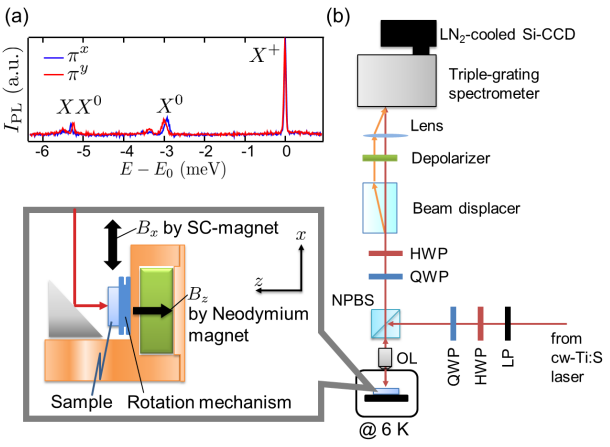

Figure 1 (a) Polarization-resolved PL spectra of a typical single InAlAs QD at 0 T under non-polarized excitation. The origin of horizontal axis is set to the energy of X^+ PL peak E_0=1.6449 eV. (b) Simultaneous measurement system of σ^+ and σ^- polarized PL components. OL: objective lens, LP: linear polarizer, HWP: half-wave plate, QWP: quarter-wave plate, NPBS: non-polarizing beam splitter. Inset: closeup view of the sample holder. The range of sample rotation angle is $0 - \sim\pi$ rad.

the blue and red lines correspond to horizontally and vertically polarized PL components (π^x, π^y). The PL peak with the highest energy has no energy splitting while the other two peaks show the same energy splitting with a reverse pattern of polarization. These facts allow us to assign each charge state as positive trion (X^+), neutral exciton (X^0), and neutral biexciton (XX^0) from the high energy side. Throughout this study, we focus on the spectra of X^+ whose ground state consists of two holes in spin singlet and one electron. In the case of X^+ PL, the degree of circular polarization (DCP) ρ_c is essentially determined only by the electron spin polarization $\langle S_z \rangle$, and thus, it can be used as a direct measure of $\langle S_z \rangle$. Here, the DCP is defined as

$$\rho_c = (I^- - I^+)/(I^- + I^+), \tag{1}$$

where I^- (I^+) is the PL intensity of σ^- (σ^+) component, and the relation ρ_c=$2\langle S_z \rangle$ is held exactly. In addition, X^+ PL is appropriate for precise evaluation of an Overhauser shift (OHS) which is the energy shift induced by the nuclear field, and it is probed by the energy difference between σ^+ and σ^- PL peaks. This is because the X^+ state is free from the exciton fine structures caused by the electron-hole exchange interaction.

In the Hanle effect measurements, we observed the DCP and OHS under a transverse magnetic field $|B_x|$ up to $\sim$1.2 T. In this $|B_x|$ region, the OHS is less than (or comparable to) the linewidth of PL spectra, and thus, the separate detection of σ^+ and σ^- PL components is essential for the precise evaluations of DCP and OHS. In order to reduce the measurement errors, a setup for the simultaneous acquisition of the orthogonal polarization components was developed as shown in Fig. 1(b) [15]. The excitation helicity (σ^-, σ^+) was changed by the combination of a linear polarizer, a quarter-wave plate (QWP) and a half-wave plate (HWP), where the HWP was used to correct the phase distortion of the circular polarization due to the optics in the excitation beam path. The (σ^+, σ^-) PL components were converted to (π^x, π^y) polarization by the combination of QWP and HWP, then separated spatially from each other by a beam displacer. The depolarizer placed in front of a triple-grating spectrometer resolves the unintentional error of DCP caused by the polarization dependence of grating diffraction efficiency. Each displaced PL component was focused on a different area of a Si-CCD detector, and then, the DCP and OHS could be evaluated accurately by a single exposure process.

Throughout this work, we performed the Hanle effect measurements at 6 K, where B_x was swept at the rate of ±0.1 T/min and the exposure time of the CCD detector was 1 s. Further, a small neodymium magnet was set to apply a longitudinal magnetic field B_z as shown in the inset of Fig.1 (b). Brief description including the magnitude and direction of B_z that the observed single QDs feel actually at 6 K will be seen in Section 4.

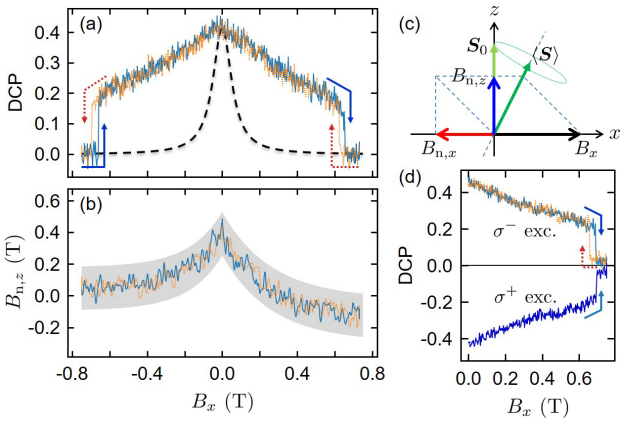

Figure 2 (a) Anomalous Hanle curve observed in a single SA InAlAs QD under σ^- excitation. The curve with increasing (decreasing) B_x is depicted as the solid (dotted) lines. Dashed curve indicates an expected normal Hanle curve with a measured g_e (=0.38) and a typical value of T_s (= 0.5 ns). (b) Out-of-plane nuclear field $B_{n,z}$. Shaded area represents twice the standard deviation of the measured value. (c) Schematics of the effective magnetic fields on electron spin $\langle \boldsymbol{S} \rangle$. (d) Anomalous Hanle curves under σ^- and σ^+ excitations.

3 Azimuth angle dependence of the anomalous Hanle curve From the Bloch equation, the steady state of electron spin polarization $\langle \boldsymbol{S} \rangle$ in the total magnetic field $\boldsymbol{B}_T^{(e)}$ is written as

$$\langle \boldsymbol{S} \rangle = \frac{(\boldsymbol{S}_0 \cdot \boldsymbol{B}_T^{(e)})\boldsymbol{B}_T^{(e)} + B_{1/2}(\boldsymbol{B}_T^{(e)} \times \boldsymbol{S}_0) + B_{1/2}^2 \boldsymbol{S}_0}{B_{1/2}^2 + \boldsymbol{B}_T^{(e)} \cdot \boldsymbol{B}_T^{(e)}}, \tag{2}$$

where $\boldsymbol{S}_0$ is the initial value of the photo-injected electron spin and $B_{1/2} = \hbar/(g_e \mu_B T_s)$ is the half width at half maximum of a Lorentzian Hanle curve (called a normal Hanle curve, hereafter) determined by the electron g factor g_e and electron spin life time T_s. Here, $\hbar$ and μ_B are the Dirac constant and the Bohr magneton, respectively. Since $\boldsymbol{S}_0$ is parallel to z axis due to the normal incidence of the excitation light, one yields $\langle S_z \rangle$ as

$$\langle S_z \rangle = S_0 \frac{B_{1/2}^2 + B_{T,z}^{(e)\,2}}{B_{1/2}^2 + \boldsymbol{B}_T^{(e)} \cdot \boldsymbol{B}_T^{(e)}}, \tag{3}$$

which corresponds to the experimentally accessible Hanle curve with the relation $\rho_c = 2\langle S_z \rangle$. The presence of a nuclear field $\boldsymbol{B}_n$ deforms the curve with a Lorentzian shape through the change of $\boldsymbol{B}_T^{(e)}$ as replacing $\boldsymbol{B}_x$ by $\boldsymbol{B}_x + \boldsymbol{B}_n$.

Figure 2(a) shows the Hanle curve observed in a single SA InAlAs QD without B_z. In the figure, a dashed curve indicates a calculated normal Hanle curve which is free from the effect of $\boldsymbol{B}_n$. Obviously, the observed curve is distorted drastically from a normal one. The anomalous broadening indicates the presence of the in-plane nuclear field $B_{n,x}$ which develops with compensating for B_x until the critical field B_c where the abrupt change in ρ_c occurs [11,12]. The value of B_c depends on the sweep direction of B_x; $|B_c|$ with increasing $|B_x|$ was larger than that with decreasing $|B_x|$. This hysteretic response is considered to originate from the bistable nature of the in-plane NSP $\langle I_x \rangle$ as the case of well-known out-of-plane NSP $\langle I_z \rangle$ [16–20]. These features in Hanle curves were observed not only in the specific QDs but in all of the studied QDs.

The observed value of $|B_c|$ increased with the excitation power density and saturated eventually [12]. This indicates that $|B_c|$ is limited by the time when unpaired electron occupies a QD, and the saturation of $|B_c|$ is synchronized with the saturation of the PL intensity. In this paper, we set the excitation power as the saturation range of the PL intensity.

Figure 2(b) shows the out-of-plane nuclear field $B_{n,z}$ deduced from the energy splitting ΔE between σ^- and σ^+ PL peaks. With the out-of-plane electron g factor $g_{e,z}$, the relation $B_{n,z} = \Delta E/(g_{e,z}\mu_B)$ is held under $B_z = 0$. The change of $B_{n,z}$ was relatively slow while the traditional model predicts a steep decay in the range of $\sim$1 mT [1], which corresponds to the dipolar interaction among the nuclear spin ensemble. The gradual decay of $B_{n,z}$ is one of key points to explain the large $B_{n,x}$ formation. Considering the spin transfer via the collinear HFI, which requires simultaneous spin flips between electron and nuclear spins, the development of $B_{n,x}$ following B_x requires a finite x component $\langle S_x \rangle$ of electron spin polarization to fulfill the momentum conservation.

According to Eq. (2), $\langle S_x \rangle$ is written as

$$\langle S_x \rangle = S_0 \frac{B_{T,z}^{(e)} B_{T,x}^{(e)} + B_{1/2} B_{T,y}^{(e)}}{B_{1/2}^2 + \boldsymbol{B}_T^{(e)} \cdot \boldsymbol{B}_T^{(e)}}. \tag{4}$$

Since only the component of $\boldsymbol{B}_n$ along the effective field on nuclei is preserved, the y component of $\boldsymbol{B}_n$, $B_{n,y}$, is considered to be very small [1,11]. In this situation where $B_{T,y}^{(e)}$ is negligible, the finite $\langle S_x \rangle$ calls for a non-zero value of $B_{T,z}^{(e)}$. Therefore, $\boldsymbol{B}_n$ must have the z component $B_{n,z}$ [Fig. 2(c)], and it was actually confirmed as shown in Fig. 2(b). Since $B_{n,z}$ originates from the out-of-plane component of NSP $\langle I_z \rangle$, the relaxation of $\langle I_z \rangle$ due to the nuclear spin precession by B_x is an issue for the formation of a large $B_{n,z}$. This can be settled by considering the stabilization of $\langle I_z \rangle$ thanks to the enhanced NQI in SA QDs [11, 21]

It is worth noting that the anomalies in Hanle curves mentioned above remain despite the change of the excitation helicity (i.e. the sign of S_0) as shown in Fig. 2(d). Although the the sign of DCP was reversed according to the definition [Eq. (1)], the overall features of the Hanle curves were identical including the gradual decay of $B_{n,z}$; the sign of $B_{n,z}$ was also reversed reflecting the sign inversion of S_0.

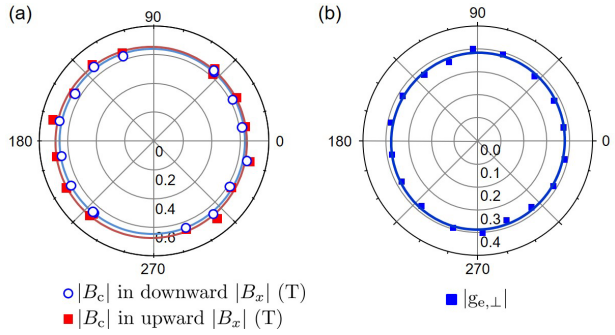

Figure 3 (a) Polar plot of $|B_c|$ for the upward (solid squares) and downward (open circles) sweeps versus azimuth angle of B_x in the laboratory frame. Solid curves are guides for eyes. (b) Polar plot of $|g_{e,\perp}|$. The solid curve is the fitting by sine function.

Figure 3(a) shows a polar plot of $|B_c|$ for the upward and downward sweeps as a function of the azimuth angle ϕ_B of B_x. Note that ϕ_B is the angle in the laboratory frame. As clearly shown, the large $|B_c|$ was almost constant for each ϕ_B. Further, we measured the in-plane electron g factor $|g_{e,\perp}|$ of the QD and confirmed that it was isotropic as shown in Fig 3(b). Therefore, the behavior of B_c can be attributed directly to the effect of NQI without worrying about the anisotropy of $|g_{e,\perp}|$. These findings allow us to consider the principal axis of NQI and its origin.

According to Ref. [1], the NQI originating from the random alloying in GaAlAs bulks (random replacement of Ga by Al atom) induces the deformation and bistability of Hanle curve in the small B_x region ($\leq \pm 2B_{1/2}$). In this case, however, since the principal axes of NQI lie along Al-As bonds (third order axes of $\langle 111 \rangle$), the deformation depends on ϕ_B strongly. As shown in Fig. 3(a), the substantial deformation of the Hanle curve in the SA InAlAs QD was almost insensitive to ϕ_B. It implies that the principal axis of NQI is not in the sample growth plane (xy plane) but along the sample growth axis (z axis), and the residual strain has a larger contribution to NQI than the random alloying in the SA InAlAs QD. This consideration is consistent with the previous reports of the Hanle measurements in a strain-free GaAs QD [13] and NMR studies in the single SA InP and InGaAs QDs [22,23].

4 Effect of an external longitudinal field in anomalous Hanle curves In this section, we use a constant B_z by a neodymium magnet in addition to the variable B_x by a superconducting magnet as shown in the inset of Fig. 1(b). The neodymium magnet has a cylindrical shape with diameter of 7 mm and height of 4 mm. The actual field strength at the QD position was evaluated from the Zeeman splitting of X^+ PL spectra. Figure 4(a) shows the energy splitting ΔE between σ^- and σ^+ PL components as a function of $\langle S_z \rangle$, where the excitation polarization was changed systematically and B_z was applied while B_x=0. Here, $\Delta E = E_{\sigma^-} - E_{\sigma^+}$, where $E_{\sigma^\pm}$ is the $\sigma^\pm$ PL peak energy. Owing to the creation of $B_{n,z}$, ΔE was modulated by changing the excitation polarization. Because the value of ΔE at $\langle S_z \rangle$=0 can be described as $(g_{e,z}+g_{h,z})\mu_B B_z$, $B_z = -265 \pm 1.4$ mT was deduced from the fitting shown as a solid curve [24]. This value is comparable to the strength of NQI (the reduced quadrupolar field B_Q as $\sim$280 mT) estimated from an independent experiment [15].

The Hanle curves with the fixed B_z are shown in Fig. 4(b). The shaded area represents the Hanle curves of the same QD under σ^+ and σ^- excitations without B_z, which have almost the same shape with reversed signs. The remarkable point is that the application of B_z broke the symmetry; the anomalies were kept under σ^- excitation while they disappeared under σ^+ excitation. Further, the absolute value of DCP at B_x=0 increased for both σ^- and σ^+ excitations. This is because B_z suppressed the decay of $\langle S_z \rangle$ caused by the nuclear spin fluctuation and helped to keep the initial value of $\langle S_z \rangle$ [25,26].

In order to explain these observations in Fig. 4(b), we deal with the effective magnetic field on nuclei explicitly as shown in Fig. 4(c) and (d), which is consistent with the general scenario based on the Bloch equation, nuclear spin cooling theory [1], and/or our proposed model [11]. First, the steady state of NSP has a part proportional to $(\boldsymbol{I}_0 \cdot \boldsymbol{B}_T^{(n)})\boldsymbol{B}_T^{(n)}$. Here, $\boldsymbol{I}_0$ is the initial value of NSP and $\boldsymbol{B}_T^{(n)}$ is a total effective field on nuclei. This part is a preserved portion of NSP which does not precess around $\boldsymbol{B}_T^{(n)}$ because it is parallel to $\boldsymbol{B}_T^{(n)}$. Considering the spin transfer to nuclei via the collinear HFI, $\boldsymbol{I}_0$ is proportional to $\langle \boldsymbol{S} \rangle$, and thus the reversal of the excitation helicity results in the sign inversion of $I_{0,z}$.

If B_z=0 as shown in Fig. 4(c), the z component of $\boldsymbol{B}_T^{(n)}$ is determined only by the Knight field $\boldsymbol{B}_e$ ($\sim$ 1 mT) which is always opposite to $\langle \boldsymbol{S} \rangle$ [1,3,27]. The excitation-helicity reversal induces the sign inversion of $B_{T,z}^{(n)}$ via the sign inversion of $B_{e,z}$, and the sign of $I_{0,z}$ is also reversed. By comparing the left and right panels of the figure, one may notice that the configuration of the NSP and effective fields on nuclei just turns upside down by changing the excitation helicity. Therefore, the NSP parallel to $\boldsymbol{B}_T^{(n)}$ has always the in-plane component which is opposite to B_x under both excitations. This is why the excitation-helicity independence of the anomalies was observed as shown in Fig. 2(d) and the shaded areas in Fig. 4(b).

In contrast, if B_z larger than $|\boldsymbol{B}_e|$ is applied like our experiments, the direction of $B_{T,z}^{(n)}$ does not depend on the excitation helicity, and is determined only by B_z as shown in Fig. 4(d). In this case, since the sign of in-plane NSP depends on the excitation helicity; $B_{n,x}$ under σ^+ excitation is parallel to B_x and increases the in-plane component of $\boldsymbol{B}_T^{(n)}$, while $B_{n,x}$ under σ^- excitation is anti-parallel to B_x and decreases $B_T^{(n)}$. Consequently, the bistable behavior was disappeared under the σ^+ excitation and re-

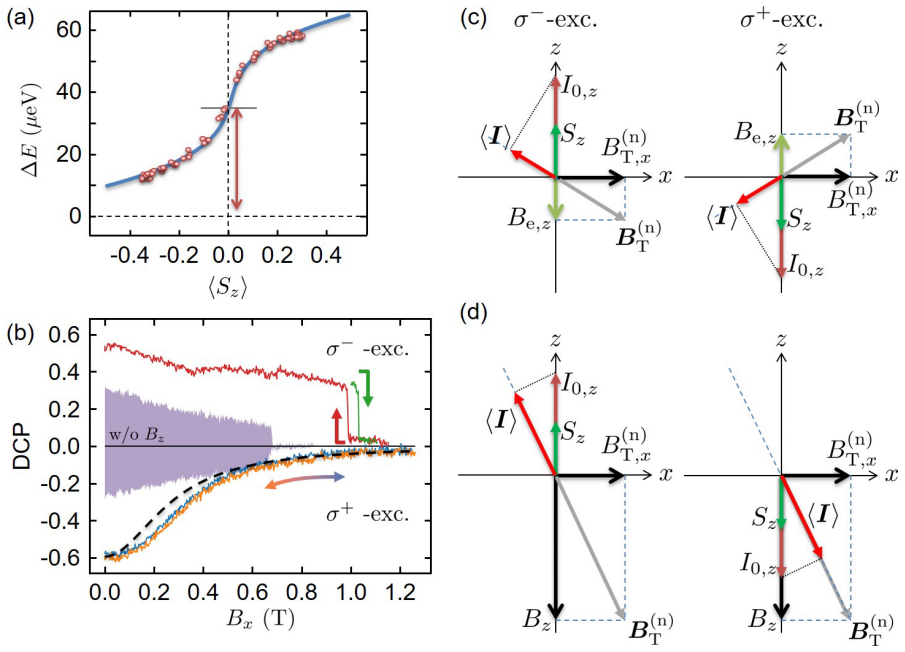

Figure 4 (a) $\langle S_z \rangle$ dependence of Zeeman splitting ΔE of X^+ PL under only a fixed B_z. The fitting by model calculation is indicated by a solid line. (b) Hanle curves under σ^- and σ^+ excitations with $B_z \sim -265$ mT. Shaded area indicates the anomalous Hanle curve without B_z which did not depend on the excitation helicity. (c) and (d) Inclination of NSP $\langle \boldsymbol{I} \rangle$ due to the effective magnetic field is illustrated. (c) and (d) indicate the cases without and with $B_z (> B_{\mathrm{e}})$, respectively. In (c) and (d), left (right) panels are the case of $\sigma^{-(+)}$ excitation.

mained under the σ^- excitation. The experiments with a similar scenario were performed in InGaAs QD ensemble by Kuznetsova *et al.* [28]. Although their Hanle effect measurements were carried out in the regime $|B_x| < 20$ mT where the traditional model was applicable, it was shown that the direction of a small $B_{\mathrm{n},x}$ is reversed by changing the direction of B_z.

Finally, the relative strength of NQI against the Zeeman interaction by B_z in this experiment is discussed. Even without considering B_{n}, the observed Hanle curve under σ^+ excitation can be reproduced approximately. The calculated Hanle curve with B_z and without the effect of B_{n} is plotted by the dashed curve in the lower panel of Fig. 4(b). From Eq. (3), it is obvious that the shape of Hanle curve with a fixed B_z is Lorentzian function as well, whose half width is given as $\sqrt{B_{1/2}^2 + B_z^2}$. Consequently, it is not strange that the broadened curve is obtained. According to this idea, it is also reasonable that the width B_{c} of anomalous Hanle curve under σ^- excitation became larger than that without B_z.

Here, in order to discuss the effect of NQI, we would like to introduce the broadening ratio, which is defined as a ratio between the width under $B_{\mathrm{n}}=0$ and that under $B_{\mathrm{n}} \neq 0$. In the case of $B_z=0$, the expected value of $B_{1/2}$ was ~ 50 mT and the width of anomalous Hanle curve $\sim B_{\mathrm{c}}$ was larger than 600 mT. Then, the broadening ratio was larger than 12. In the case with B_z on the other hand, the normal Hanle curve is ~ 270 mT and the observed value of B_{c} under σ^- excitation is ~ 1 T. Therefore the broadening ratio was only about 3 and reduced to one quarter compared to the case of $B_z=0$. Although the introduction of B_z may strongly assist the $B_{\mathrm{n},x}$ formation via the enhancement of $\langle S_x \rangle$ intuitively, the maximal value of B_{c} seems to be determined by the material properties like the strength of NQI fundamentally and independent of the external condition such as B_z. Since the NQI originates from the couping to the electric field gradient around nucleus, a magnetic field in any direction cannot modulate the NQI directly. Thus, there is no contradiction with the idea that the maximal value of B_{c} which is a benchmark of $B_{\mathrm{n},x}$ is determined by NQI. The above consideration implies that the formation of large $B_{\mathrm{n},x}$ cannot be explained by only the emergence of $\langle S_x \rangle$, and thus, the NQI plays not only the stabilizer of NSP but also other roles on the generation of $B_{\mathrm{n},x}$. Our proposed model actually assumes the strong anisotropy in the magnetic response of nuclei as well as the NSP stabilization [11]. In order to support this scenario, more detailed discussion dealing with the eigenstates of nuclear spins explicitly is necessary. Since it seems to be possible to modulate the eigenstate ordering by varying B_z, similar experiments under various B_z will yield deep insight into the effect of NQI from microscopic viewpoint.

5 Conclusions We investigated the role of NQI via the anomalous Hanle effect in single self-assembled QDs where the in-plane nuclear field developed compensating for the applied B_x. It was revealed that the critical field B_{c} was almost insensitive to the azimuth angle of B_x. This isotropic feature of B_{c} suggests that the principal axis of the NQI is close to the sample growth axis (z axis). Therefore, the residual strain in QDs has major contribution to the in-plane nuclear field formation via the NQI compared with the random alloying in InAlAs. Further, an additional longitudinal magnetic field B_z induced clear changes in the Hanle curves depending on the excitation helicity, which

could be explained with a simple consideration. While it has a stabilization effect on the electron and nuclear spins along the z axis as well as NQI, our analysis based on the broadening ratio indicates that the maximal value of in-plane NSP is determined mainly by the material properties like the strength of NQI and insensitive to the experimental conditions.

Acknowledgements This work is supported by JSPS KAKENHI (Grant No. 17K19046) and The Hattori Hokokai Foundation.

References

[1] *Optical Orientation*, Modern Problems in Condensed Matter Sciences Vol. 8, Chaps. 2 and 5, edited by F. Meier and B. Zakharchenya. North-Holland, NewYork, **1984**.
[2] *Spin Physics in Semiconductors*, Springer Series in Solid-State Sciences Vol. 157, edited by M. I. Dyakonov. Springer, Berlin, **2008**.
[3] Recent optical investigation of nuclear spin physics in QDs are reviewed comprehensively: B. Urbaszek, X. Marie, T. Amand, O. Krebs, P. Voisin, P. Maletinsky, A. Högele, A. Imamoglu, *Rev. Mod. Phys.* **2013**, *85*, 79.
[4] B. E. Kan, *Nature (London)* 1998, *393*, 133.
[5] J. M. Taylor, C. M. Marcus, M. D. Lukin, *Phys. Rev. Lett.* **2003**, *90*, 206803.
[6] *Optical Generation and Control of Quantum Coherence in Semiconductor Nanostructures*, edited by G. Slavcheva and P. Roussignol. Springer-Verlag, Berlin, **2010**.
[7] C. Boehme, D. R. McCamey, *Science* **2012**, *336*, 1239.
[8] D. A. Gangloff, G. Éthier-Majcher, C. Lang, E. V. Denning, J. H. Bodey, D. M. Jackson, E. Clarke, M. Hugues, C. Le Gall, M. Atatüre, *Science* **2019**, *364*, 62.
[9] O. Krebs, P. Maletinsky, T. Amand, B. Urbaszek, A. Lemaître, P. Voisin, X. Marie, A. Imamoglu, *Phys. Rev. Lett.* **2010**, *104*, 056603.
[10] J. Nilsson, L. Bouet, A. J. Bennett, T. Amand, R. M. Stevenson, I. Farrer, D. A. Ritchie, S. Kunz, X. Marie, A. J. Shields, B. Urbaszek, *Phys. Rev. B* **2013**, *88*, 085306.
[11] S. Yamamoto, R. Matsusaki, R. Kaji, S. Adachi, *Phys. Rev. B* **2018**, *97*, 075309.
[12] R. Kaji, S. Yamamoto, R. Matsusaki, and S. Adachi, *Jpn. J. Appl. Phys.* **2019**, *58*, SBBH10.
[13] G. Sallen, S. Kunz, T. Amand, L. Bouet, T. Kuroda, T. Mano, D. Paget, O. Krebs, X. Marie, K. Sakoda, B. Urbaszek, *Nat. Commun.* **2014**, *5*, 3268.
[14] T. Yokoi, S. Adachi, H. Sasakura, S. Muto, H. Z. Song, T. Usuki, S. Hirose, *Phys. Rev. B* **2005**, *71*, 041307(R).
[15] R. Matsusaki, R. Kaji, S. Yamamoto, H. Sasakura, S. Adachi, *Appl. Phys. Express* **2018**, *11*, 085201.
[16] B. Eble, O. Krebs, A. Lemaître, K. Kowalik, A. Kudelski, P. Voisin, B. Urbaszek, X. Marie, T. Amand, *Phys. Rev. B* **2006**, *74*, 081306(R).
[17] P.-F. Braun, B. Urbaszek, T. Amand, X. Marie, O. Krebs, B. Eble, A. Lemaître, P. Voisin, *Phys. Rev. B* **2006**, *74*, 245306.
[18] A. I. Tartakovskii, T. Wright, A. Russell, V. I. Fal'ko, A. B. Van'kov, J. Skiba-Szymanska, I. Drouzas, R. S. Kolodka, M. S. Skolnick, P. W. Fry, A. Tahraoui, H.-Y. Liu, M. Hopkinson, *Phys. Rev. Lett.* **2007**, *98*, 026806.
[19] P. Maletinsky, C. W. Lai, A. Badolato, A. Imamoglu, *Phys. Rev. B* **2007**, *75*, 035409.
[20] R. Kaji, S. Adachi, H. Sasakura, S. Muto, *Phys. Rev. B* **2008**, *77*, 115345.
[21] R. I. Dzhioev, V. L. Korenev, *Phys. Rev. Lett.* **2007**, *99*, 037401.
[22] E. A. Chekhovich, K. V. Kavokin, J. Puebla, A. B. Krysa, M. Hopkinson, A. D. Andreev, A. M. Sanchez, R. Beanland, M. S. Skolnick, A. I. Tartakovskii, *Nat. Nanotech.* **2012**, *7*, 646.
[23] E. A. Chekhovich, M. Hopkinson, M. S. Skolnick, A. I. Tartakovskii, *Nat. Commun.* **2015**, *6*, 6348.
[24] The following parameters are used in the calculations: we assumed that $g_{e,z}=+0.34$, $g_{h,z}=-2.57$, $\tilde{A}_z=52.6$ μeV, $N=3\times10^4$, where $g_{e(h),z}$ is the out-of-plane electron (hole) g-factor, $\tilde{A}_z$ is an averaged hyperfine constant, and N is a number of atoms in a QD, respectively. The fitting results were $f_eT_{ND}=0.25$ ms, $\tau_c=50.0$ ps, and $B_z=-265\pm1.4$ mT, where f_e, T_{ND}, τ_c are the time fraction the unpaired electron occupies the QD, the correlation time, and the magnetic field by a neodymium magnet, respectively.
[25] I. A. Merkulov, Al. L. Efros, M. Rosen, *Phys. Rev. Lett.* **2002**, *65*, 205309.
[26] R. Kaji, S. Adachi, H. Sasakura, S. Muto, *Phys. Rev. B* **2012**, *85*, 155315.
[27] P. Maletinsky, doctoral thesis, Swiss Federal Institute of Technology, Zurich, **2008**.
[28] M. S. Kuznetsova, K. Flisinski, I. Ya. Gerlovin, I. V. Ignatiev, K. V. Kavokin, S. Yu. Verbin, D. R. Yakovlev, D. Reuter, A. D. Wieck, M. Bayer, *Phys. Rev. B* **2013**, *87*, 235320.